View Article Online / Journal Homepage / Table of Contents for this issue
Dynamic Article Links

Soft Matter

Cite this: *Soft Matter*, 2011, **7**, 5329

www.rsc.org/softmatter

PAPER

Structuring of colloidal suspensions confined between a silica microsphere and an air bubble

Yan Zeng and Regine von Klitzing*

Received 14th December 2010, Accepted 28th March 2011
DOI: 10.1039/c0sm01487g

Published on 27 April 2011. Downloaded by TU Berlin - Universitaetsbibl on 01/04/2016 09:21:16.

This study contributes to the understanding of the effects of confining surface properties on the interactions within thin liquid films of colloidal nanoparticles. Colloidal probe atomic force microscopy was used for studying the interaction of colloidal nanoparticles between the solid–liquid and air–liquid interfaces. The influence of the surfactant on the surface deformability and on the structuring of the nanoparticles was determined. Therefore, surfactants of different charges, *i.e.* sodium dodecyl sulfate (SDS), hexadecyltrimethylammonium bromide ($C_{16}TAB$) and β-dodecylmaltoside (β-$C_{12}G_2$) were chosen. The oscillatory force caused by the layering formation of the nanoparticles was detected between the AFM microsphere probe and the bubble, and the oscillatory wavelength that reflected the interlayer distance of the nanoparticles was found to scale with colloidal nanoparticle concentration as $c^{-1/3}$. Under constant experimental conditions (AFM probe radius, bubble size, Debye length and contact angle), the bubble stiffness was found to increase linearly with surface tension, while the oscillatory wavelength was not affected by the bubble's deformability. In addition, the cationic surfactant $C_{16}TAB$ displayed different behavior on the retraction part of the force curve, in which a pronounced adhesion force was observed. This phenomenon might be attributed to the hydrophobization caused by the monolayer formation of cationic surfactant on the silica sphere surface. Thus a stable thin film of colloidal nanoparticles was assumed to be formed between the silica microsphere and the bubble when electrostatic repulsion existed.

1 Introduction

Large numbers of chemicals and consumer products such as polymeric latexes, paints, inks, coatings, cosmetics and lotions, foams, gels or emulsions depend on the colloid suspension quality and structuring of colloidal suspensions. It is also apparent that the control of industrial processes like sedimentation, flocculation and coagulation for the manufacture of advanced self-assembled materials can be greatly improved by understanding of the factors that affect the quality and stability of colloidal suspensions. The structuring and stability of colloidal suspensions depend highly on the interaction forces between the colloidal nanoparticles and the confining surfaces.

The classic Derjaguin–Landau–Verwey and Overbeek (DLVO) theory balances the repulsive electrostatic double layer and the attractive van der Waals forces between colloidal nanoparticles. This theory has been found to be useful in enabling scientists and engineers to develop industrial products and processes that employ colloidal suspensions. However, in recent years, due to the advent of new instruments, such as atomic force microscopes,[1–3] surface force apparatus,[4,5] thin film pressure balances[6–9] and total internal reflection microscopes,[10,11] for measuring interaction forces in colloidal suspensions, a non-DLVO force, known as the oscillatory structural force, arising due to the entropic excluded volume effect, has been characterized.[4] Oscillatory force becomes apparent when colloidal nanoparticles are confined in the gap between two smooth macroscopic surfaces. When the separation distance between two macroscopic surfaces is on the order of several colloidal nanoparticle diameters, the colloidal nanoparticles interact with the macroscopic surfaces and tend to form parallel layers. This long-range ordering induces a repulsive structural barrier which helps to prevent the macroscopic particles from flocculating or coalescing. When the separation distance between macroscopic surfaces is smaller than the diameter of the colloidal nanoparticles, no nanoparticles can fit in the gap between macroscopic surfaces and a net attractive force, known as a depletion force, is expected due to the osmotic pressure difference between film and reservoir (meniscus). In general, the interaction induced by the nanoparticles between two macroscopic surfaces is found to be oscillatory in length dimensions. The wavelength of oscillation is equal to the spacing of the ordered layers of colloidal nanoparticles and the amplitude of oscillation is the strength of

Stranski-Laboratorium für Physikalische und Theoretische Chemie, Institute for Chemistry, Technical University Berlin, 10623 Berlin, Germany. E-mail: klitzing@mailbox.tu-berlin.de; Fax: +49-(0)30-314-26602; Tel: +49-(0)30-314-23476

View Article Online

Published on 27 April 2011. Downloaded by TU Berlin - Universitaetsbibl on 01/04/2016 09:21:16.

the ordering. Thus we can understand the structuring of nanoparticles by studying the oscillatory force.

Many studies have reported the stability and layered structuring of colloidal nanoparticles confined between two solid macroscopic surfaces by atomic force microscopy.[12–14] In general, AFM measurements of colloidal particles trapped between a silica microsphere and a flat silica wafer show that the oscillatory force becomes more pronounced with increasing particle size, increasing particle concentration and increasing confining surface charge while the oscillatory wavelength decreases solely with increasing particle concentration. The comparisons between the structuring of silica nanoparticles in thin films and in the volume phase has been studied as well.[15,16] The colloidal nanoparticles confined between two silica surfaces form ordered layers and the oscillatory wavelengths scale with particle concentration as an exponent of $-1/3$ and give the same values as the mean particle distance in the volume phase. In addition, Monte Carlo simulations with a Grand Canonical Potential show that the interaction between charged nanoparticles in confined geometries can be described by a DLVO potential and give results consistent with experimental ones.[15–19]

However, there are only a few pieces of work that report the interaction between colloid particles such as micelles or latex particles[6–9] confined between deformable surfaces like in a foam lamella. Typically, a thin film pressure balance (TFPB) is used. The existence of oscillatory forces is detected by a sequence of steps in film thickness. The step size between two adjacent repulsive branches, which is connected to the layering distance or the oscillatory wavelength, is found to be comparable to the effective particle diameter, including the Debye length, at relatively high particle concentrations. This is different from the AFM results obtained between two solid surfaces. Thus the effect of surface deformability on the layering phenomenon needs to be taken into account.

In this study, a direct force measurement of silica nanopaticles between a silica microsphere and a bubble was performed by using colloidal probe atomic force microscopy. The surface deformability was tuned by varying the type and amount of surfactants and the effect of surface deformability on the structuring of colloidal nanoparticles was investigated.

2 Experimental

2.1 Preparation of colloidal nanoparticle suspensions

Ludox grade TMA colloidal silica nanoparticle suspensions (TMA 34 wt%, deionized, Aldrich, Germany) were used in AFM force measurements. The original stock of colloidal suspensions was dialyzed with Milli-Q water (Millipore, Billerica, MA, USA) for two weeks. The dialysis tubes (Aldrich, Germany) with MWCO of 1000 were used to remove any remaining ions and ionic contaminants. After dialysis, particle suspensions of varying concentrations were prepared with Milli-Q water as the solvent. The weight percentage of the solutions were determined by weighing the sample before and after drying (24 h at 400 °C). The particle size was determined by scanning electron microscopy (SEM, S-4000, Hitachi, Japan) at a primary electron energy of 20 keV and atomic force microscopy with tapping mode with a multimode nanoscope (Digital Instruments, CA). The average particle diameter was 25 ± 2 nm compared to the manufacturer-quoted value of 22 nm.[20] The ζ-potential was determined by electrokinetic measurements (Zeta Sizer, Malvern) at the same conditions employed in the AFM experiments. The measured ζ-potential at PH ≈ 7 without adding extra salts was -60 ± 5 mV.

2.2 Preparation of surfactants

β-Dodecylmaltoside (β-$C_{12}G_2$) (Glycon), sodium dodecyl sulfate (SDS) (Sigma-Aldrich, purity >99.9%) and hexadecyltrimethylammonium bromide (C_{16}TAB) (Sigma-Aldrich, purity >99%) were used as received. The critical micelle concentrations are 0.17 mM, 8 mM, and 1 mM for β-$C_{12}G_2$, SDS, and C_{16}TAB, respectively. All surfactant solutions were prepared with Milli-Q water. The surfactant concentrations were always well below the cmc.

2.3 Preparation of AFM silica sphere surface

A silica sphere (Bangslabs, USA) with radius of $R = 3.35$ μm was glued with epoxy glue (UHU Endfest Plus 300) at the end of a tipless rectangular cantilever (CSC12, MikroMasch, Estonia) using a three-dimensional microtranslation stage according to the previously reported procedure.[1] Immediately before each experiment the silica sphere with cantilever was cleaned by exposure to a plasma cleaner for 20 min to remove all the organic contaminants and to create a high density of hydrophilic silanol groups (Si–OH) on the surface.

2.4 Preparation and attachment of air bubble on hydrophobic surface

A Teflon slide was cleaned in concentrated nitric acid for several minutes, followed by thorough rinsing with Milli-Q water. Air bubbles were spontaneously transferred from an eppendorf pipette onto the bottom of a Teflon slide which was immersed in Ludox nanoparticle suspensions. The bubble diameter was typically 800 μm as determined by top view microscope connected to an AFM. Gas bubbles are thermodynamically unstable and tend to dissolve in water due to the Laplace pressure.[21] However air bubbles are much more stable in colloidal nanoparticle suspensions, probably because the particles act as emulsifiers of air and water and prevent coalescence of bubbles.[22]

2.5 Force measurements

The cantilever was placed into a cantilever holder and the particle was positioned roughly a few μm above the bubble. Fig. 1 shows the schematic of AFM setup with top view image of cantilever placing on the top of the bubble. Deflection-*vs*-Zsensor curves were measured with a commercial atomic force microscope MFP produced by Asylum Research, Inc. and distributed by Atomic Force (Mannheim, Germany). With this instrument the position of the cantilever was controlled and determined by a *z*-axis position sensor equipped with the piezoelectric translator and the cantilever deflection was determined from the motion of the laser-beam reflected from the back of the microfabricated silicon cantilever. The spring constant of each cantilever was individually determined by thermal noise power spectra before or after the experiment,[23] which yielded values in the range 0.01–0.045 N m^{-1}.

 This journal is © The Royal Society of Chemistry 2011

View Article Online

Published on 27 April 2011. Downloaded by TU Berlin - Universitaetsbibl on 01/04/2016 09:21:16.

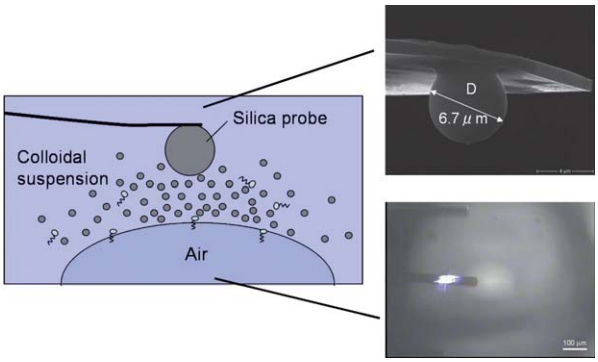

Fig. 1 Left: schematic representation of the AFM setup for the force measurements. Right top: scanning electron microscope image showing the silica microsphere glued to the end of the AFM cantilever. Right bottom: view from the top showing placement of cantilever probe right on the top centre of the air bubble surface. The middle cantilever at which the laser beam aligned is in focus. The brightest part of the ring underneath is the top centre of the bubble.

The scanning frequencies were varied from 0.5 to 1 Hz over a scan size of 300–400 nm, which corresponded to approach velocities in the range of 150–400 nm s^{-1}. Chan and Engel showed that hydrodynamic drainage forces were negligible at these approach speeds.[24,25] For each sample solution, 30–40 force–distance curves in total were recorded at the same lateral position (usually at the centre) with respect to the air–water interfaces.

2.6 Analysis

Firstly, it is necessary to calibrate the deflection inverse optical lever sensitivity (InvOLS), which is the sensitivity of the detector–cantilever combination. Most previous experiments have involved solid substrates that are much stiffer than the cantilevers. The deflection InvOLS can thus be simply calibrated by finding the slope of deflection *vs.* Zsensor once the surfaces are in contact. In the present case the cantilever and bubble can have similar stiffnesses so that the calibration must be done separately, before or after the force measurements, by pressing the particle against a rigid surface. The conversion from the raw data into force-*vs*-distance plots was performed as in the protocol of Ducker *et al.*[2] The AFM photodiode voltage was converted to cantilever deflection using the detector sensitivity determined before the experiment and then converted to force via

$$F = k_c Z_c \tag{1}$$

where k_c is the spring constant of the cantilever and z_c is the deflection of the cantilever.

The conversion from Zsensor position to actual particle–bubble separation is more complicated. The nominal separation is defined as

$$\Delta X = \Delta z_c - \Delta z_p \tag{2}$$

where Δz_p is the Zsensor position. This definition does not consider deformation, so for rigid surfaces the nominal separation coincides with the actual separation. For deformable surfaces, the actual separation is the nominal separation minus the deformation

$$\Delta S = \Delta X - \Delta\delta \tag{3}$$

An attractive force between AFM probe and substrate causes an extension and a positive deformation while a repulsive force causes a negative deformation. During the measurements an absolute measure of the shape change of the bubble surface is not known, only the changes in ΔX are measured. This problem cannot be resolved without measurement of actual particle–bubble separation using an independent method, *e.g.* interferometry. Thus it is difficult to plot F *vs.* S. Instead F *vs* ΔX is presented in this paper.

$$\Delta X = \Delta S + \Delta\delta \tag{4}$$

The 'contact point' (zero ΔX) was taken to be the point at which the linear compliance line reached zero force, followed by the previous protocols on deformable surfaces.[26,27] Before contact, ΔX represents the separation plus the relatively small deformation of the bubble which depends on the surface force between the probe and the bubble. After contact, ΔX represents only the deformation of the bubble because the separation between the probe and the bubble surface is considered to be zero. In the constant compliance region, the cantilever and the bubble are assumed as two springs in a series where the measured stiffness k_m is given by

$$\frac{1}{k_m} = \frac{1}{k_c} + \frac{1}{k_b} \tag{5}$$

The bubble stiffness is given by

$$k_b = \frac{k_c}{\frac{k_c}{k_m} - 1} = \frac{k_c}{\frac{C_{hard}}{C_{bubble}} - 1} \tag{6}$$

where C_{hard} is the cantilever optical lever sensitivity against a hard surface and C_{bubble} is the cantilever optical lever sensitivity against the bubble.

The bubble stiffness can be also calculated by

$$k_b = \frac{F_b}{\delta} = \frac{F}{\delta} \tag{7}$$

since for two springs in series, $F = F_b = F_c = k_b \times \delta = k_c \times z_p$.

Attard described a theoretical way to express the stiffness of bubble or droplet with

$$k = \frac{-4\pi\gamma}{\frac{\cos\theta}{2+\cos\theta} + \ln\left[\frac{R}{2\kappa R_b^2} \times \frac{(1+\cos\theta)^2}{\sin^2\theta}\right]} \tag{8}$$

which showed that the bubble stiffness linearly depended on the surface tension γ, and logarithmically depended on the decay length of the interaction κ^{-1}, the radius of the bubble R_b, the radius of the probe R and the contact angle θ.[28,29]

To quantitatively study the structuring of nanoparticles, the oscillatory forces were fitted with

$$\frac{F(x)}{R} = A\exp\left(-\frac{x}{\xi}\right)\cos\left(2\pi\frac{x}{\lambda} + \theta\right) + \text{offset} \tag{9}$$

The three important parameters characterizing the oscillations are the amplitude A, the wavelength λ, and the decay length ξ.[16,30] Force per cantilever radius $\frac{F(x)}{R}$ is the measure of interaction

View Article Online

Published on 27 April 2011. Downloaded by TU Berlin - Universitaetsbibl on 01/04/2016 09:21:16.

energy per area. Because the silica microsphere is 6.7 μm in diameter and bubble is 800 μm in diameter, by the Derjaguin approximation both surfaces can be considered as flat surfaces because of the comparatively small force distance (<300 nm). All experimental force curves were fitted with eqn (9). Beside the three mentioned parameters a phase shift (θ) and a force offset (offset) also had to be fitted.

3 Results

3.1 Force profiles in the absence of additives

The result of a force experiment between a hydrophilic silica microsphere and a bubble in Milli-Q water without extra electrolytes is shown in Fig. 2. There, the force is plotted *versus* relative separation ΔX (change in separation and deformation of the bubble as aforementioned). At ΔX larger than 400 nm, no force was detected and the ΔX was considered as the pure separation between the silica probe and the initial bubble surface because soft particles behave as rigid ones when there is no surface force at a large distance.[31] A monotonic repulsion began to appear when the probe further approached the bubble. This repulsion is at least partially caused by the electrostatic double layer force because the silica probe is negatively charged and the air–water interface is slightly negatively charged as well.[32–34] The decay length determined in the linear region of the inset logarithmic plot was 102 nm, which agreed with the expected value of the Debye screening length ($\kappa^{-1} = 96$ nm at an ionic strength of 10^{-5} M for pure water).

When the probe was moved further toward the bubble, the force increased linearly while remaining within the so-called constant compliance region. On solid surfaces, the separation between the silica probe and the substrate does not change in the constant compliance region and the increase of force is due to the consistent bending of the cantilever after contacting the solid surface. On the bubble surface we can assume that the separation between the probe and the bubble surface in the constant compliance region does not change either because a stable water film is formed between the silica probe and air.[26] Thus ΔX represents only the deformation of the bubble in the constant compliance region (eqn (4)). The deviation of force direction from the vertical observed on rigid surfaces is due to the deformation of the bubble from its equilibrium shape. The slope of force *versus* ΔX at negative ΔX region ($F/\Delta X$) could be used as another measure of the bubble stiffness since $F = k_b\Delta\delta = k_b\Delta X$.

The bubble stiffness of a 800 μm diameter bubble in water calculated from eqn (6) or eqn (7) is typically $k_b = 76$ mN m^{-1} which is only two times larger than the spring constant of cantilevers used in the force measurements. Therefore, considering bubble deformation is necessary when measuring forces against bubbles with such soft cantilevers.

3.2 Colloidal nanoparticle suspensions in the absence of surfactants

The normalized force *versus* ΔX curves for a silica probe interacting with a bubble surface in TMA nanoparticle suspension at varying particle concentrations is shown in Fig. 3. When the distance was larger than 200 nm, no force could be detected. The oscillatory force, or structural force of nanoparticles, grew more intense during the approach and resulted from the mutual repulsion between the nanoparticles and the layer-by-layer expulsion of the nanoparticles.

The oscillatory wavelengths, which represent the distances between two adjacent nanoparticle layers, decreased with increasing nanoparticle concentrations. This parameter was defined as the distance between successive force maxima or minima. At the same time, the oscillations increased in amplitude at the higher concentrations because the nanoparticles were forced closer to each other, resulting in stronger electrostatic repulsion.

Following the oscillatory force, an attractive depletion force was observed due to the exclusion of all particles from the confined gap between the silica probe and bubble. Additionally,

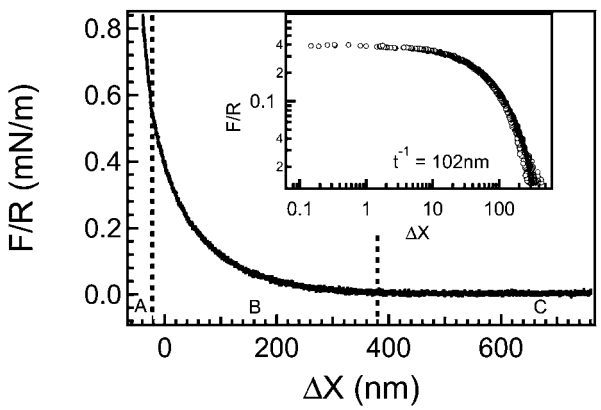

Fig. 2 Normalized force (F/R) *versus* ΔX curves of a silica microsphere and an air bubble in water. 'A' presents the constant compliance region where the loading force is linearly increased; 'B' presents the surface force region between the silica microsphere and the bubble; 'C' presents the region where no surface force is detected. The monotonical decay region is fitted with a decay length of 102 nm in the inset graph with double logarithmic scale.

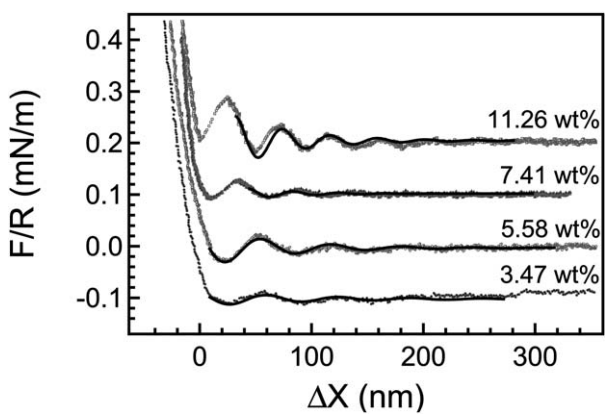

Fig. 3 Normalized force (F/R) *versus* ΔX curves of a silica microsphere and an air bubble at different Ludox TMA suspensions (3.47 wt%, 5.58 wt%, 7.41 wt%, 11.26 wt%). The solid lines are the corresponding curves fitted to eqn (9). The force profiles have been offset vertically for ease of viewing.

 This journal is © The Royal Society of Chemistry 2011

View Article Online

Published on 27 April 2011. Downloaded by TU Berlin - Universitaetsbibl on 01/04/2016 09:21:16.

at small separations, an electrostatic repulsive force between confining surfaces appeared, which decayed to zero at larger separation as the nanoparticle concentration decreased.

3.3 In the presence of non-ionic surfactants

β-$C_{12}G_2$ is a non-ionic surfactant which adsorbs at the air–water interface resulting in a decrease in the surface tension. The adsorption of β-$C_{12}G_2$ to negatively charged silica has been shown to be weak.[35,36] The deformation of the bubble at the same nanoparticle concentration with varying β-$C_{12}G_2$ concentration is illustrated in Fig. 4a. The slope of the force in the constant compliance region decreased with increasing β-$C_{12}G_2$ concentration. The surface tension of the bubble decreased from 72 mN m^{-1} to 50 mN m^{-1} at 5×10^{-5} M β-$C_{12}G_2$ and to 40 mN m^{-1} at 10^{-4} M β-$C_{12}G_2$, and the corresponding bubble stiffness was 44 mN m^{-1} and 35 mN m^{-1}, respectively. The decrease in the bubble stiffness, or increase in deformability was caused by the decrease of interfacial tension and can be understood by means of eqn (8).

The force profiles as shown in Fig. 4b were fitted with eqn (9) in order to obtain the quantitative values of oscillatory wavelength and amplitude. The oscillatory wavelengths showed no change after adding different amounts of β-$C_{12}G_2$ surfactant into the nanoparticle suspensions. A decrease in oscillatory amplitude with increasing β-$C_{12}G_2$ surfactant concentration was observed due to the reduced surface stiffness and surface charge. (Detailed discussions see section 4.2.) The pure air–liquid interface is assumed to be negatively charged[34] and the β-$C_{12}G_2$ molecules partially replace the negative charges. A decrease in surface charge leads to a reduction of the oscillatory amplitude as previously shown by us,[17] in which it is also shown that a modification of the charge, or potential of the confining surfaces has no effect on the oscillatory wavelength.

The force profiles of at 5×10^{-5} M β-$C_{12}G_2$ at different nanoparticle concentrations are shown in Fig. 5. The oscillatory amplitude increased with nanoparticle concentration while the oscillatory wavelength decreased since the nanoparticles were closer at higher concentrations. This behavior was the same as in the absence of added surfactant.

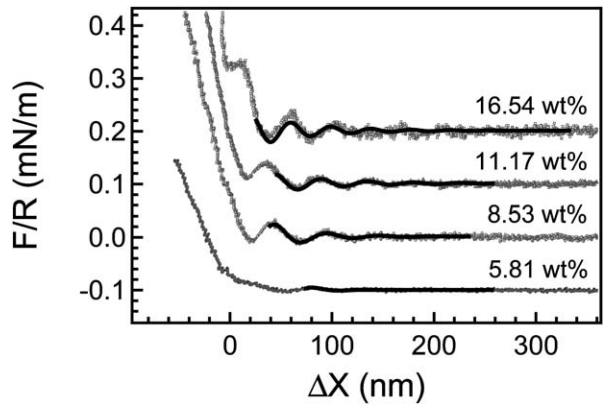

Fig. 5 Interaction between a silica microsphere and an air bubble at 5.81 wt%, 8.53 wt%, 11.17 wt% and 16.54 wt% Ludox TMA suspension with 5×10^{-5}M β-$C_{12}G_2$. The solid lines are the corresponding curves fitted to eqn (9). The force profiles have been offset vertically for ease of viewing.

3.4 In the presence of anionic surfactants

Sodium dodecyl sulfate is an anionic surfactant which only adsorbs at the air–water interface. A stable film of nanoparticles was formed between the silica probe and the bubble in this case as well, and the repulsive force at the constant compliance region was also observed and attributable to the electrostatic double layer force. The bubble stiffness slightly increased to 80 mN m^{-1} although the interfacial tension did not show measurable change at this concentration of SDS in comparison to that of pure water (Fig. 6). This can be explained according to eqn (8) which expresses the effect of the decrease of Debye length on the increase of the bubble stiffness. Charged SDS brings extra dissociated ions into the suspension, thus leading to a decrease of the Debye length. An increase of the oscillatory amplitude in the nanoparticle force profile was observed for two reasons. In addition to the slightly increased surface stiffness, it was also likely that it is due to dodecyl sulfate ions adsorbing at the air–water interface and the increase of the interfacial effective charge.[17] Hence, we would expect an increase in the electrostatic

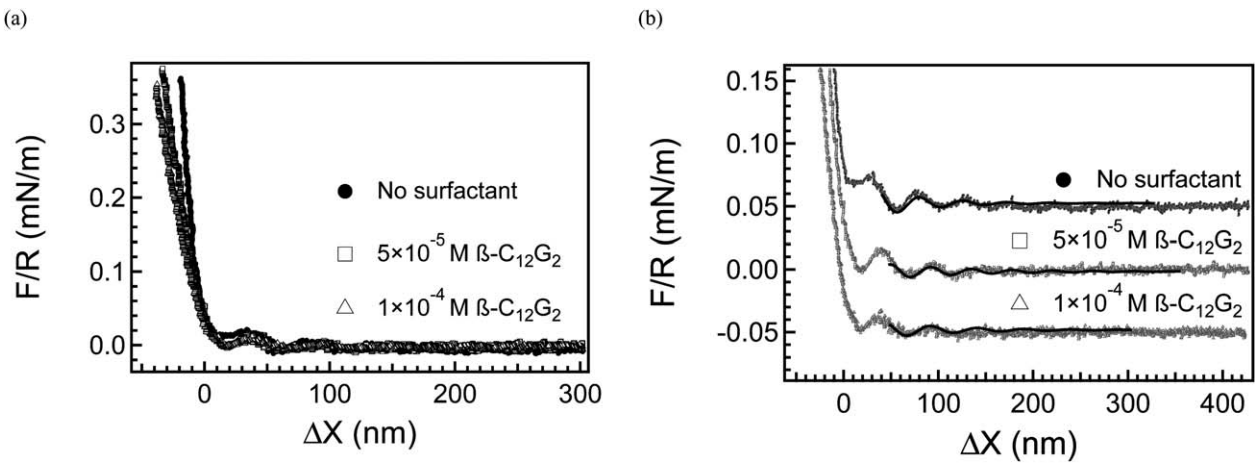

Fig. 4 (a) Interaction between a silica microsphere and an air bubble at 9 wt% silica nanoparticle suspensions and different β-$C_{12}G_2$ concentrations (0 M, 5×10^{-5} M, 10^{-4} M). (b) The force profiles have been offest vertically for ease of comparison of oscillatory forces. The solid lines are the corresponding curves fitted to eqn (9). (Details see Section 2.6.)

View Article Online

Published on 27 April 2011. Downloaded by TU Berlin - Universitaetsbibl on 01/04/2016 09:21:16.

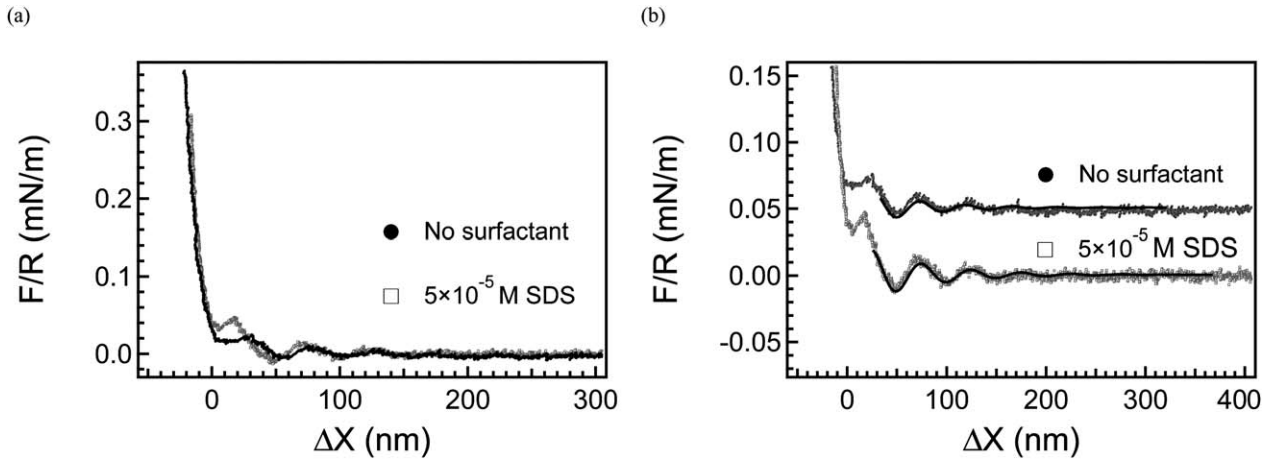

Fig. 6 (a) Interaction between a silica microsphere and an air bubble at 9 wt% Ludox TMA suspensions with 5×10^{-5} M of SDS and without any surfactant. (b) The force profiles have been offset vertically for ease of viewing. The solid lines are the corresponding curves fitted to eqn (9).

double layer force with increasing SDS concentration up to the critical micelle concentration (cmc).[37] The oscillatory wavelengths obtained after quantitative fitting were found to remain the same compared to the previous cases without surfactants and with β-$C_{12}G_2$.

3.5 In the presence of cationic surfactants

Unlike SDS and β-$C_{12}G_2$, hexadecyltrimethylammonium bromide is a cationic surfactant which not only strongly adsorbs at air–water interfaces, but also at silica microsphere and nanoparticle surfaces, due to interaction of opposite charges on the silica surface and the cationic surfactant head group.

The contact angle measurements of $C_{16}TAB$ on a silica wafer shown in Fig. 7 displayed an increase of contact angle to a maximum at around 0.05 mM followed by a decrease again with further increase of $C_{16}TAB$, which indicated that a monolayer of $C_{16}TA^+$ was formed on the silica wafer at a concentration of 0.05 mM.[38] While at this concentration, the adsorption of $C_{16}TAB$ on the bubble surface was very low and only led to a reduction in surface tension of approximately 1.5%.

Based on the contact angle measurement, we expected to measure attractive forces due to adsorption of $C_{16}TA^+$ on the silica probe. A snap into the bubble often occurred in $C_{16}TAB$ solution during manual approach, which increased the difficulty of measurement. An example is shown in Fig. 8 when the full piezo range was used in the experiment. A jump-to contact appeared during the approach and a large adhesion force existed during retraction and no jump-off from the contact was observed. The jump-to contact and the adhesion took place due to the hydrophobic attractive force between the $C_{16}TA^+$ adsorbed silica probe and the bubble. However, once nanoparticles were added, the long-range oscillatory force induced a repulsive structural barrier which helped to overwhelm the hydrophobic attraction by forming layers between the silica probe and the bubble. Thus the AFM force curves in such concentrations of $C_{16}TAB$ containing silica nanoparticles could be recorded.

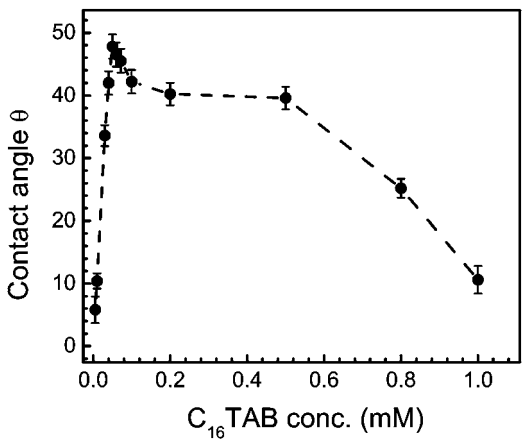

Fig. 7 The contact angle of $C_{16}TAB$ on silica wafer as a function of surfactant concentration. The maximum of the contact angle appears at a concentration of 0.05 mM resulting from the monolayer formation of the cationic surfactant on the negatively charged silica wafer surface. The further decrease of the contact angle is because of the bilayer formation of the surfactant and re-hydrophilization the silica surface.

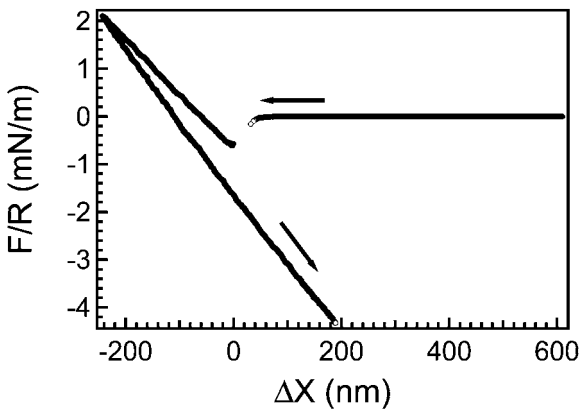

Fig. 8 Interaction between a silica microsphere and an air bubble at 5×10^{-5} M of $C_{16}TAB$ solution without colloidal nanoparticles. A jump into contact appears during approach and a large adhesion force exists during retraction.

 This journal is © The Royal Society of Chemistry 2011

View Article Online

Published on 27 April 2011. Downloaded by TU Berlin - Universitaetsbibl on 01/04/2016 09:21:16.

Fig. 9a shows that an oscillatory force began to be detected at around 200 nm and was present until a separation of 30 nm and then a repulsive force in the constant compliance region was detected at smaller ΔX. When the probe was retracted from the bubble, an adhesion force appeared instead of the oscillatory force between nanoparticles. The reason for the different behaviors on approach and retraction might be due to the different surfactant structure at air–liquid interfaces. During the approach of the probe to the bubble, the monolayer of $C_{16}TA^+$ adsorbed on the silica microsphere surface underwent desorption because of the increasing surface force between the probe and the bubble. Thus the surface of the silica probe behaved as a non-adsorbed hydrophilic surface and a stable film of nanoparticles existed in between. When retracting the two surfaces, $C_{16}TA^+$ began to adsorb on the probe surface due to the reduction of the surface force, thus the attractive force appeared between two hydrophobic surfaces. The advancing contact angle could be calculated from

$$\cos\theta_a = \frac{R - D}{R} \tag{10}$$

where D is the jumping off distance.[39]

The advancing contact angle varied greatly in each force measurement with a maximum of 35° observed, which was smaller than the contact angle measured on the planar silica wafer in the equilibrium state. This phenomenon was probably due to the unstable organization process of cationic surfactant adsorbed to the silica when the surfactant concentration was below the cmc. The slow adsorption of cationic surfactant was reported by Parker *et al.*[40] and Fleming *et al.*,[41] who found that the build-up of the CTAB layer on a silica surface became more rigid with time.

Fig. 9b shows the oscillatory forces in the presence and absence of $C_{16}TAB$. The oscillatory wavelengths in both cases remained constant. This further indicates that the layering distance of nanoparticles in the confinement is particle number density determined, even though the surface charge of the nanoparticles was reduced after the adsorption of oppositely charged surfactants. The force slope at negative ΔX was lower than in the corresponding case in the absence of surfactant, meaning that the deformability of the bubble increased after adding 5×10^{-5} M of $C_{16}TAB$, even though the interfacial tension at this concentration was just slightly smaller than that of water. The bubble stiffness was 59 mN m^{-1}, which was attributed to the change in the contact angle as described in eqn (8).

In comparison to the absence of surfactant, a reduction of force amplitude was observed. The reasons were most likely the decreased surface stiffness, and the reduced surface charge both on bubble surface and nanoparticle surfaces.

4 Discussion

4.1 The effect of surface tension on the deformability of the air–liquid interface

In contrast to the deformation of elastic and viscoelastic materials which is controlled by the bulk materials properties, the deformation of bubbles (air–liquid interface) is controlled by the surface tension and the pressure across the interface. The deformation, or elasticity, of the air–liquid interface is typically measured by the oscillating bubble/droplet method. Here, AFM force measurement provides a direct way to determine the deformation of the bubble by assuming that it behaves as a Hookean spring under the force applied by the AFM probe. Although some theoretical papers doubt the validity of this assumption,[42,43] Attard *et al.*[28] and Chan *et al.*[44] concluded that a Hookean force law is valid for weak forces ($F/2\pi R \ll \gamma$). The existence of the constant compliance region with a linear slope in the force curves is evidence of linear elasticity for the fluid interface.

The deformability can be expressed as the bubble stiffness by eqn (6), or directly from the slope of force curves in the negative ΔX region with eqn (7). The values of the bubble stiffness, surface tension, oscillatory wavelength, and the oscillatory amplitude at varying Ludox TMA and surfactant concentrations are summarized in Table 1. The increase in the Ludox concentration did not cause significant change in the surface stiffness of the bubble. This was due to the negligible change in the air–liquid

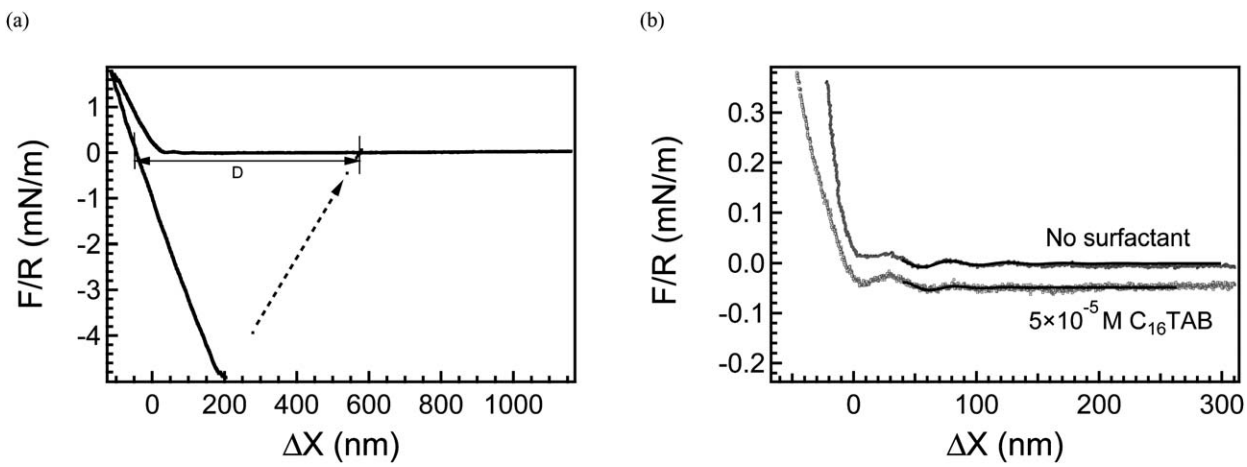

Fig. 9 (a) Interaction between a silica microsphere and an air bubble in 9 wt% TMA suspensions with 5×10^{-5} M of $C_{16}TAB$. The oscillatory force of the nanoparticles appears during the approach while a pronounced adhesion force appears during retraction. '*D*' denotes the distance of jumping off contact which is used to calculate the advancing contact angle. (b) The oscillatory forces in the presence and absence of $C_{16}TAB$ are compared. The force profiles have been offset for ease of viewing. The solid lines are the corresponding curves fitted to eqn (9).

View Article Online

Published on 27 April 2011. Downloaded by TU Berlin - Universitaetsbibl on 01/04/2016 09:21:16.

Table 1 Summary of the surface tension γ from tensiometer measurements, the bubble stiffness k_b calculated from force curves and the oscillatory wavelength λ and amplitude A of force curves

Surfactant conc. [M]	Ludox conc. [wt%]	γ [mN m^{-1}]	k_b [mN m^{-1}]	λ [nm]	A [mN m^{-1}]
0	0	71.8	76.7	—	—
	3.47	71.5	75.9	67.8	0.0130
	5.58	71.7	77.0	64.8	0.0373
	7.41	71.9	76.4	54.2	0.0478
	9.00	72.0	75.8	49.6	0.0564
	11.26	72.9	72.7	48.2	0.1018
5×10^{-5} C $_{12}G_2$	5.81	49.7	—	60.7	0.0095
	8.53	49.2	48.1	54.9	0.0253
	9.00	50.2	44.2	50.0	0.0517
	11.17	49.8	45.8	48.2	0.0708
	16.54	50.1	47.3	41.4	0.1115
1×10^{-4} C $_{12}G_2$	9.00	40.1	34.7	50.9	0.0448
5×10^{-5} SDS	9.00	71.5	79.8	50.1	0.0660
5×10^{-5} $C_{16}TAB$	9.00	70.6	59.3	50.9	0.0500

interfacial tension with an increase in the particle concentration, although the Debye length of the aqueous solution did decrease. Thus we can assume the effect of the Debye length on the surface stiffness of the bubble is relatively small.

At a given Ludox concentration (9 wt%), the plot of the experimental bubble stiffness *versus* surface tension is shown in Fig. 10a. The square points were obtained from the system with β-$C_{12}G_2$. The increase of β-$C_{12}G_2$ concentration led to the linear decrease of the surface tension. The circle point (SDS) lies along the linear fit because the surface stiffness was not significantly influenced by the decrease of Debye length after adding charged surfactants into this solution. On the other hand, the data for $C_{16}TAB$ (triangle point) deviated from the linear fit because of the increase of the contact angle after the adsorption of $C_{16}TAB$ on the probe surface.

Thus the linear dependency of the bubble stiffness on the air–liquid interfacial tension is valid if the following conditions remain constant: probe radius, bubble radius, Debye length, and the contact angle. This is consistent with the theoretical expression in eqn (8). Also from eqn (8), one should expect that surface tension and the contact angle play a more important role than bubble size and Debye length, which explains why the decrease in Debye length introduced by the increase of nanoparticle concentration has a negligible effect on the surface stiffness. In addition, the contact angle is strongly associated with the air–liquid interfacial tension, which further supports that the deformation of fluid interfaces is surface tension controlled.

4.2 The effect of surface deformability on the structuring of nanoparticles

At constant nanoparticle concentration (9 wt%), the oscillatory force amplitude exhibited an increase with the bubble surface stiffness. (Fig. 10b) In the present study, the change of the surface deformability was always associated with the change of the surface charge. Studying the system with non-ionic surfactant β-$C_{12}G_2$, we were unable to analyze both factors in force amplitude independently, because surface charge and surface stiffness both decreased with increasing surfactant concentration. The reduced surface stiffness and surface charge mutually caused the reduction of force amplitude. Studying anionic

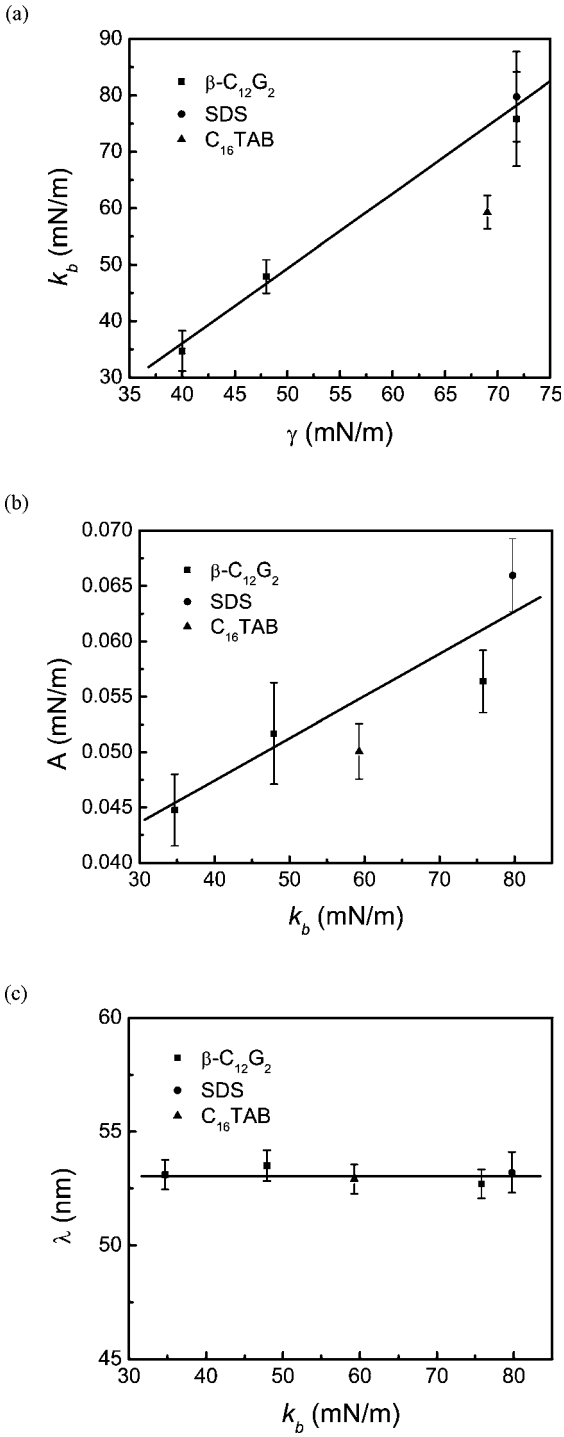

Fig. 10 The relationship of the bubble stiffness with the surface tension (a) and with the corresponding oscillatory amplitude (b) and oscillatory wavelength (c) at 9 wt% TMA colloidal nanoparticle suspensions.

surfactant SDS was expected to hopefully shed some light on the two parameters since the increase of surfactant concentration led to an increase of the surface charge. However, a slight increase of the surface stiffness was observed as well, which had the same effect on the change of the force amplitude as surface charge did. Thus the separation of these two causes was also difficult. In the case of cationic surfactant $C_{16}TAB$, an additional complication

 This journal is © The Royal Society of Chemistry 2011

View Article Online

Published on 27 April 2011. Downloaded by TU Berlin - Universitaetsbibl on 01/04/2016 09:21:16.

was introduced resulting from the interaction between the surfactant and the oppositely charged nanoparticle surface. Therefore, the force amplitude could be considered as the joint consequence of the electrostatic and rigidity effects.

At constant nanoparticle concentration (9 wt%), the oscillatory wavelength, representing the layering distance of nanoparticles, showed no dependency on the bubble stiffness or surface deformability. (Fig. 10c) With regard to the case of cationic surfactant, the oscillatory wavelength did not show any difference even though the surface charge of nanoparticles was additionally reduced.

The log–log dependence of AFM oscillatory wavelengths *versus* nanoparticle concentrations is summarized in Fig. 11. Wavelengths obtained from measurements of AFM probe of the deformable air–liquid interface in the presence and absence of β-$C_{12}G_2$ surfactants were compared to that of a solid silica wafer. For all cases, the oscillatory wavelength scaled with the nanoparticle concentration as an exponent of -0.33, which agreed very well with the purely space-filling value of $-1/3$. This indicated that nanoparticles under such confinement formed a layering pattern where the interparticle distances scaled to 1/3 of the total volume of nanoparticles. These results were in good agreement with recent experimental and theoretical results by Klapp *et al.*[16] and Fazelabdolabadi *et al.*,[19] which were based on non-deformable silica surfaces. The experimental findings indicate that the deformability of the confining surfaces does not change the layering packing pattern of particles in between. The particle distance remains the same and solely depends on the particle concentration, or particle number density regardless of the confinement type. The strength of ordering, however, decreases with increasing surface deformability associated with change of the surface charge.

The difference in wavelengths between the system with the deformable bubble surface and corresponding system with a solid surface was only approximately 1%. This supports the reliability of using force *versus* ΔX curves in determining the particle layering distance, even though the deformation of the bubble surface contributes at smaller distances.

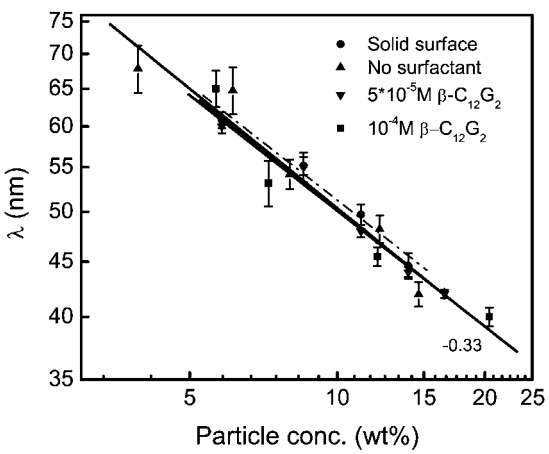

Fig. 11 The log–log plot of oscillatory wavelengths *versus* Ludox TMA concentrations against the air–liquid interface without surfactant, with 5×10^{-5} M of β-$C_{12}G_2$, with 10^{-4} M of β-$C_{12}G_2$, and against a solid silica wafer. Values of oscillatory wavelengths on solid silica wafer were determined from published force curves.[16]

5 Conclusions

AFM provided a direct way to study the structuring of silica nanoparticles confined between a deformable air–water interface and a rigid solid surface. The air–water interface deformability increased with decreasing surface tension and could be observed directly from the change of force slope at the constant compliance region of force profiles.

The layering distance and the force strength between nanoparticles could be obtained from the wavelength and the amplitude of the oscillatory force, respectively. It was found that the oscillatory wavelength was not affected by the surface deformability (associated with surface charge) and was the same as between two solid surfaces, while the force amplitude decreased with increasing surface deformability associated with surface charge. It is worth mentioning that, for cationic surfactant (C_{16}TAB), a different behavior was displayed on the retraction part of the force curve, in which a pronounced adhesion force appeared. Different surfactant structures were assumed to exist in the approaching and retracting processes. Thus a stable thin film of colloidal nanoparticles was assumed to be formed between the silica microsphere and the bubble when electrostatic repulsion existed.

The fact that the surface properties (surface deformability, surface charge) had no effect on the oscillatory wavelength further proved that the layering distance depended solely on the particle concentration. In contrast to this, the ordering strength was found to depend on the surface properties as well, thus it was affected not only by nanoparticle concentration, but also by the surface deformability and surface charge after adding extra surfactants.

Acknowledgements

We thank Ulrich Gernert, Zelmi TUBerlin, for scanning electron images of the AFM probe. We further acknowledge financial support of the Deutsche Forschungsgemeinschaft *via* SPP 1273 "Kolloidverfahrenstechnik" (KL1165/10-2).

References

1 W. Ducker, T. Senden and R. Pashley, *Nature*, 1991, **353**, 239–241.
2 W. Ducker, T. Senden and R. Pashley, *Langmuir*, 1992, **8**, 1831–1836.
3 H. Butt, *Biophys. J.*, 1991, **60**, 1438–1444.
4 J. Israelachvili and R. Pashley, *Nature*, 1983, **306**, 249–250.
5 P. Richetti and P. Kekicheff, *Phys. Rev. Lett.*, 1992, **68**, 1951–1954.
6 V. Bergeron and C. Radke, *Langmuir*, 1992, **8**, 3020–3026.
7 A. Nikolov and D. Wasan, *J. Colloid Interface Sci.*, 1989, **133**, 1–12.
8 P. Kralchevsky, A. Nikolov, D. wasan and I. Ivanov, *Langmuir*, 1990, **6**, 1180–1189.
9 A. Nikolov and D. Wasan, *Langmuir*, 1992, **8**, 2985–2994.
10 A. Sharma and J. Walz, *J. Chem. Soc., Faraday Trans.*, 1996, **92**, 4997–5004.
11 A. Sharma, S. Tan and J. Walz, *J. Colloid Interface Sci.*, 1997, **191**, 236–246.
12 M. Piech and J. Walz, *J. Phys. Chem. B*, 2004, **108**, 9177–9188.
13 A. Tulpar, P. Van Tassel and J. Walz, *Langmuir*, 2006, **22**, 2876–2883.
14 C. McNamee, Y. Tsujii, H. Ohshima and M. Matsumoto, *Langmuir*, 2004, **20**, 1953–1962.
15 S. H. L. Klapp, S. Grandner, Y. Zeng and R. von Klitzing, *J. Phys.: Condens. Matter*, 2008, **20**, 494232.

View Article Online

Published on 27 April 2011. Downloaded by TU Berlin - Universitaetsbibl on 01/04/2016 09:21:16.

16 S. H. L. Klapp, Y. Zeng, D. Qu and R. von Klitzing, *Phys. Rev. Lett.*, 2008, **100**, 118303.
17 S. Grandner, Y. Zeng, R. v. Klitzing and S. H. L. Klapp, *J. Chem. Phys.*, 2009, **131**, 154702.
18 S. H. L. Klapp, S. Grandner, Y. Zeng and R. von Klitzing, *Soft Matter*, 2010, **6**, 2330–2336.
19 B. Fazelabdolabadi, J. Y. Walz and P. R. Van Tassel, *J. Phys. Chem. B*, 2009, **113**, 13860–13865.
20 A. Vanblaaderen and A. Kentgens, *J. Non-Cryst. Solids*, 1992, **149**, 161–178.
21 P. Epstein and M. Plesset, *J. Chem. Phys.*, 1950, **18**, 1505–1509.
22 B. Binks, *Curr. Opin. Colloid Interface Sci.*, 2002, **7**, 21–41.
23 J. Hutter and J. bechhoefer, *Rev. Sci. Instrum.*, 1993, **64**, 1868–1873.
24 R. Dagastine, G. Stevens, D. Chan and F. Grieser, *J. Colloid Interface Sci.*, 2004, **273**, 339–342.
25 J. Hoh and A. Engel, *Langmuir*, 1993, **9**, 3310–3312.
26 M. Fielden, R. Hayes and J. Ralston, *Langmuir*, 1996, **12**, 3721–3727.
27 H. Butt, B. Cappella and M. Kappl, *Surf. Sci. Rep.*, 2005, **59**, 1–152.
28 P. Attard and S. Miklavcic, *Langmuir*, 2001, **17**, 8217–8223.
29 P. Attard and S. Miklavcic, *Langmuir*, 2003, **19**, 2532.
30 S. H. L. Klapp, D. Qu and R. von Klitzing, *J. Phys. Chem. B*, 2007, **111**, 1296–1303.
31 G. Gillies, C. Prestidge and P. Attard, *Langmuir*, 2001, **17**, 7955–7956.
32 G. Collins, M. Motarjemi and G. Jameson, *J. Colloid Interface Sci.*, 1978, **63**, 69–75.
33 A. Graciaa, P. Creux, J. Lachaise and J. Salager, *Ind. Eng. Chem. Res.*, 2000, **39**, 2677–2681.
34 K. Ciunel, M. Armelin, G. Findenegg and R. von Klitzing, *Langmuir*, 2005, **21**, 4790–4793.
35 L. Zhang, P. Somasundaran and C. Maltesh, *J. Colloid Interface Sci.*, 1997, **191**, 202–208.
36 D. Lugo, J. Oberdisse, M. Karg, R. Schweins and G. H. Findenegg, *Soft Matter*, 2009, **5**, 2928–2936.
37 H. Schulze and C. Cichos, *Zeitschrift Fur Physikalische Chemie-Leipzig*, 1972, **251**, 252–268.
38 B. Bijsterbosch, *J. Colloid Interface Sci.*, 1974, **47**, 186–198.
39 M. Preuss and H. Butt, *Langmuir*, 1998, **14**, 3164–3174.
40 M. Rutland and J. Parker, *Langmuir*, 1994, **10**, 1110–1121.
41 B. Fleming, S. Biggs and E. Wanless, *J. Phys. Chem. B*, 2001, **105**, 9537–9540.
42 D. Aston and J. Berg, *J. Colloid Interface Sci.*, 2001, **235**, 162–169.
43 D. Bhatt, J. Newman and C. Radke, *Langmuir*, 2001, **17**, 116–130.
44 D. Chan, R. Dagastine and L. White, *J. Colloid Interface Sci.*, 2001, **236**, 141–154.

 This journal is © The Royal Society of Chemistry 2011